International Journal of Emerging Trends in Science and Technology
6 (2) December 2020, 24-30
http://www.publishingindia.com/ijetst

A Survey of Coastal Satellite Image Sensing with Estimation of Erosion and Accretion Rates using QGIS – Mapping [CSIS EEAR]

Meivel S.[1*] and Sridevi A.[2]
[1]Assistant Professor, Department of ECE, M.Kumarasamy College of Engineering, Karur, Tamil Nadu, India.
Email: meivels.ece@mkce.ac.in
[2]Professor, Department of ECE, M.Kumarasamy College of Engineering, Karur, Tamil Nadu, India.
Email: sridevia.ece@mkce.ac.in
*Corresponding Author

Abstract: This paper has proposed to utilize Remote Sensing and Geoinformation Systems (GIS) to screen and investigate the coastline morpho-dynamics during the most recent twenty years. All datasets of Arabia Coastline is from MODIS web and Landsat 7 for researching Arabia - Coastal line. Erosion and Accretion rates calculated using the Panchromatic Sharpened Algorithm and Universal Pixel Quality Index, Which implies classification of ATWT, DWT, GS, and PC algorithms. Multispectral images of the Coastal line are extracted and validated accuracy assessment. Changing Rate of Arabia coastal line measured using a digital short line analysis system.

Keywords: Image processing, QGIS, Remote sensing.

I. Introduction

The Arabia strip frames just a little segment (42 km) of a bigger Study Area coastline sunken framework (a "littoral cell") that reaches out from Alexandria at the west side of the Nile Delta through Arabia [18]. Nile waterways had a content of sunken coastal line with clockwise searching. It detected N-S-W-E wise direction changing of seawater movements [9].

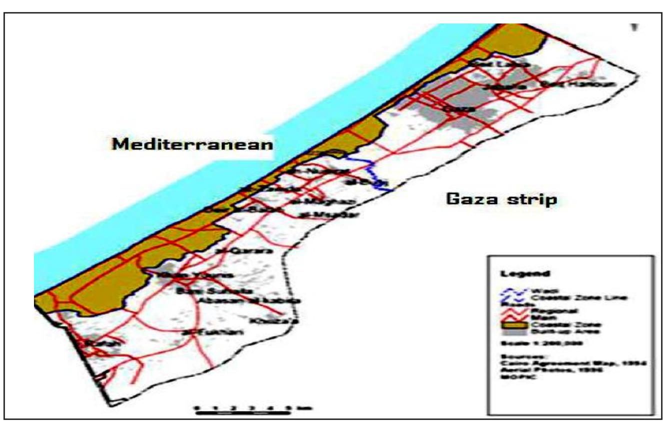

Fig. 1: Arabia Coastline Mapping Strip [17]

From Fig. 1, the sea-side zone of Arabia is one of the most seriously utilized regions and populated on the planet. Arabia coast and seashore has been changed and dirtied because of numerous reasons had including human exercises (like the Arabia seaport, power generator unit, sewage removal from the home grown's zone, drainage sewage on the seashore). From Fig. 2, the Arabia shoreline had influenced and corrupted by marine measures [4], for example, wave disintegration and statement, and flows like an alongshore current [5]. This examination had begun regardless of the deficiency season of the examines, absence of the in situ information, and incapacity to lead the hands-on work so far because of the political issue in the locale.

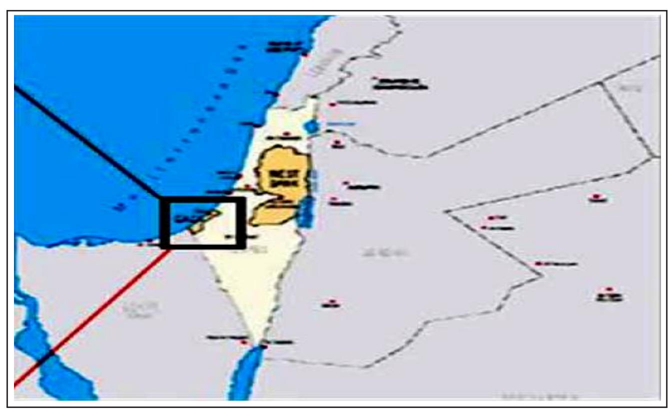

Fig. 2: Image Extraction and Masking of Coastal Line

II. Methodology Outline

IMAGES preprocessing and arrangement

- Images segmentation.
- Pixels Conversion esteem to brilliance.
- Climatic rectification utilizing F-L-A-A-S-H correction to air remedy Model.

Information combination and PAN appraisal quality and Sharpening

- Quality Pixels.
- Image enlistment (RMS 0.2-0.02).
- Coastlines programmed removing and it is a quality quality signal receiving. Computing the pace of progress in the Arabia seaside zone utilizing (Digital Shoreline Analysis System [20]), USGS.

III. Methodology: Fusion using Pan-Sharpening

High-Resolution Satellite images [7] are not accessible for the Arabia area [2] before the year 2002 and because of the restricted budgetary spending. Here could not procure costly high-goal optical symbolism. The Testing used ETM+ progression images with 30 m Landsat various points, Landsat TM with 30 m symbolism, and panchromatic images of SPOT with 5 m long-term assessments and shown its higher performance. Sensible outcome Caught in Coastal line in Arabia beach.

- Pan and sharpening quality.
- Pixel Extraction and quality assessment of Coastline imagery.
- Changed Rating Measurements.
- Panchromatic FUSION assessment and Survey.

Fig. 3: Panchromatic Image of Coastline

The Panchromatic-Quality pixels level combination method. It had used to expand Multispectral Spatial resolution utilizing Spatial images [8] in the Tif file and data in the multispectral image and Hyperspectral data calculations on ETM satellite [13] images (Fig. 3).

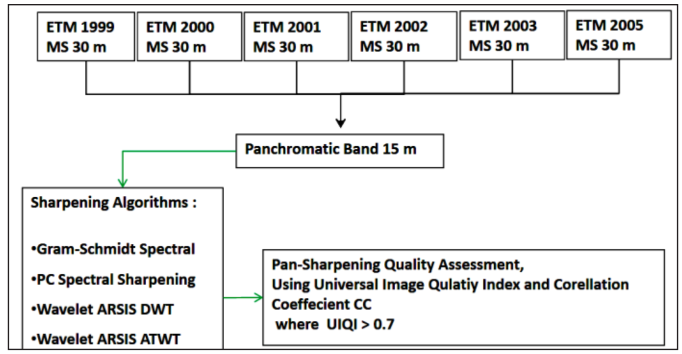

Fig. 4: Panchromatic Image Band in ETM+ with 30 m

To assess the Spatial data of Panchromatic Quality image [11] calculations (Fig. 4). The Verification of multispectral images had completed in the picture deduction of Variance Panchromatic, UIQI-Universal Image Quality Index, CC-Correlation coefficient, and characterization of hyperspectral image.

	Pan-sharpened algorithm			
	ATWT	DWT	PC	GS
Band	Mean	Mean	Mean	Mean
b1-b1	8	2,26	7,23	7,14
b2-b2	12,7	6,55	2,58	10,9
b3-b3	32,2	20,54	29,7	27,5
b4-b4	14,43	5,7	1,09	4,06
b5-b5	31,5	16,5	27,06	19,68
b7-b7	39	25,9	39,4	31,2
Aver.	22,9	12,9	17,8	16,7

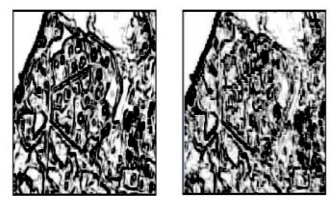

Variance image of ATWT   Variance image of DWT

Fig. 5: Panchromatic Sharpened Algorithm in Variance

Trous Wavelet remodel (ATWT) is a multiresolution stationary wavelet decomposition set of rules with marine ecosystems conversion [12]. A trous WT pan-sharpening is comparable in operation to pan-sharpening with the aid of normal WT, aside from the utilized WT. A trous WT is an undecimated wavelet transform and its low bypass clear out kernel. Burt and Adelson first evolved the Laplacian Pyramid (LP) which is derived from the Gaussian Pyramid. The ranges of Gaussian Pyramid constitute a low-skip filtered version of a photograph, respectively.

LP includes detailed snapshots which are extracted from the subtraction of the identical stage picture and its interpolated low skip model. improved LP (ELP) has been delivered via adding features that put in force zeroth degree entropy and the lower correlation. Generalized LP (GLP) is derived from ELP via adding the belongings of fractional scale variety as a ratio. In pan-sharpening by way of GLP, the pan-sharpened photograph is received after LP detail extraction from the PAN image, after which injecting information to the MS picture up-sampled to PAN decision. The Quality Image depends on the Subtraction of MS image Variance from Panchromatic image

Variance (Fig. 5). [cA, cH, cV, cD] = dwt2 (X, name) computes the single-stage 2-D discrete wavelet transform (DWT) of the enter records X using the w-name wavelet. dwt2 returns the approximation coefficients matrix cA and element coefficients matrices cH, cV, and cD (horizontal, vertical, and diagonal, respectively).

The GS spectral sharpening approach enhances the spatial decision of the MS photo by merging the excessive decision PAN photograph with the low spatial resolution. The GS fusion simulates the PAN band from the lower spatial decision spectral bands. Use PC Spectral Sharpening to sharpen a low spatial resolution multi-band image [11] the use of a related excessive spatial decision panchromatic band [8]. The algorithm assumes that the low spatial decision spectral bands corresponding to the excessive spatial decision panchromatic band.

- Universal Pixel Quality Index (UPQI)

The CC - correlation coefficient measured from variance of the panchromatic image and variance of panchromatic quality MS images. From Table I, compared ATWT Wavelet Transforms Types with coastal image datas.

Table I: Comparison of ATWT Wavelet Transforms Types

ATWT - A TRUS FILTER				DWT - DAUBECHIES WAVELET			
BAND	GEN	URBAN	AGRI	BAND	GEN	URBAN	AGRI
B1	0.8	0.65	0.72	B1	0.92	0.54	0.82
B2	0.85	0.68	0.75	B2	0.93	0.57	0.81
B3	0.87	0.68	0.75	B3	0.94	0.57	0.81
AVG	0.86	0.67	0.74	AVG	0.93	0.56	0.81
GSSS - GRAM SVHMIDT SPECTRAL SHARPENING				PCSS - PC SPECTRAL SHARPENING			
BAND	GEN	URBAN	AGRI	BAND	GEN	URBAN	AGRI
B1	0.69	0.77	0.75	B1	0.82	0.86	0.85
B2	0.74	0.72	0.74	B2	0.72	0.72	0.73
B3	0.81	0.73	0.76	B3	0.72	0.67	0.71
AVG	0.74	0.73	0.75	AVG	0.75	0.75	0.76
COMPARISION OF ALGORITHMS							
ALGS	B1	B2	B3	B4	B5	B7	B8
ATWT	0.65	0.65	0.6	0.63	0.65	0.65	0.65
DWT	0.45	0.51	0.51	0.42	0.42	0.49	0.52
PCSS	0.6	0.64	0.6	0.52	0.58	0.57	0.57
GSSS	0.6	0.64	0.59	0.59	0.53	0.52	0.52

Table II: Classification of ATWT, DWT, GS and PC

CLASSIFICATION				
ALGS	Original MS Image vs Pan Sharpened Image		Panchromatic Image Classes vs Pan Sharpened Image Classes	
	15 classes	30 classes	02 classes	05 classes
ATWT	37	70	25	36
DWT	30	64	51	57
GS	59	75	27	66
PC	71	84	15	31

From Table II, ATWT, DWT, GS, and PC Percentages of MS class changes and Panchromatic Changes calculated for finding Quality Panchromatic images.

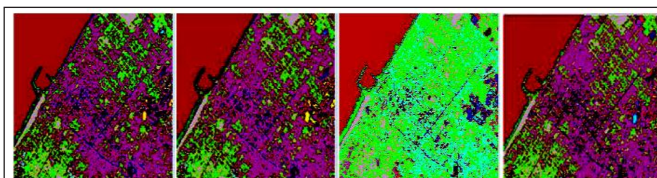

Unsupervised K-mean classification, from the left to the right: ATWT, DWT, PC and GS

Fig. 6: Unsupervised K-mean Classifications

For the most part, wavelet dish honing calculations stored the phantom data of performed - images, particularly the DWT container-honing calculation, the Spatial DATA of DWT is not different calculations for medium goal pictures. PC otherworldly and ATWA dish honing calculations acquired the quality spatial data outcomes individually (Fig. 6). ATWT transform changes had utilized to container hone the multispectral + ETM + images spatial data of 30 m to 15 m.

IV. The Methodology Depends on Extraction of Coastline Multispectral Images

From Fig. 7 and Fig. 8, the Coastline Automatic Extraction coastline is the line at the crossing Assemble point of coupling land [15] and the level plane of the adjoining ocean surface [10]. In the investigation, various strategies had been performed to the extrication coastline consequently, NDVI, TCT-Tasseled Cap Transformation (Wetness), and Band Ratio and PCA segmentation. In the process, Coastal Signal image converted and estimated the previous image datasets, which is following steps given Fig. 7 and Fig. 8.

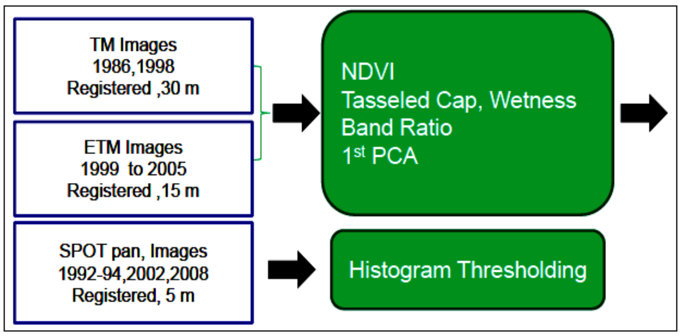

Fig. 7: TM, ETM and SPOT Images Conversion

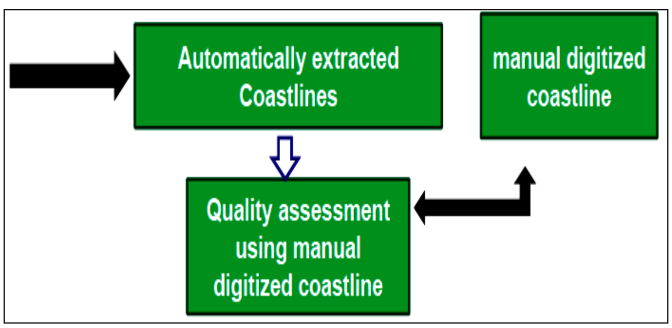

Fig. 8: Coastline Image Estimation

The digitalized coastlines had captured for each image. The coastline referenced to survey the programmed separated coastline. The issues of programmed extraction of coastline:

- Froth and waves of Seawater
- Tsunami of seawater
- Shoal of Underwater (boundaries and barriers)

The Coastline Extraction based on Accuracy Assessment (Fig. 12) determined the mean of naturally removed coastlines utilizing various techniques are PCA, NDVI, Tasseled top moistures (Fig. 12), frequency Band Ratio and finding air polluted areas in coastal [6]. The strategy had to separate the coastline consequently increased in closest to zero lines (Fig. 13). In Fig. 9, shown Seawater Foam, Waves and Sandbar for coastline extraction [Fig. 10] and accuracy results. In Fig. 11, shorted ETM 2005 Coastline.

V. Coastline Extraction: Accuracy Assessment

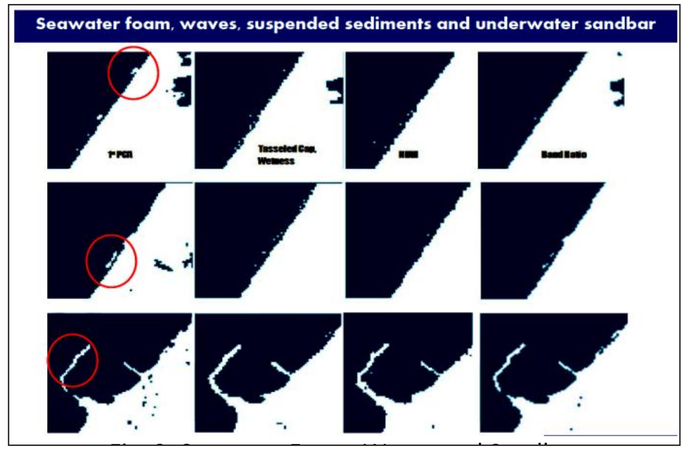

Fig. 9: Seawater Foam, Waves and Sandbar

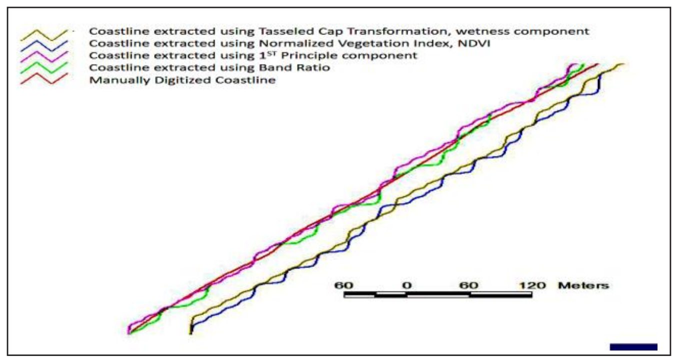

Fig. 10: Coastline Extraction in Meter

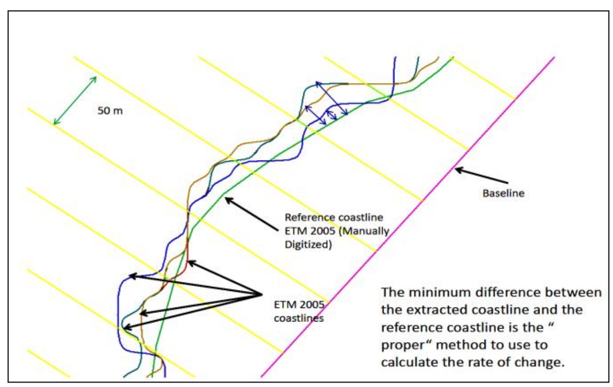

Fig. 11: ETM 2005 Coastline

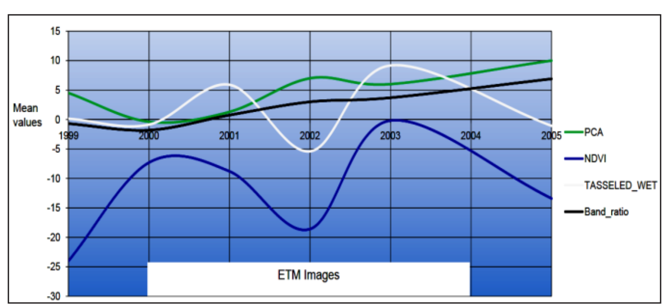

Fig. 12: ETM Images Reading Comparison from 1999 to 2005

VI. Measure the Changing Rate through Arabia Coastal Line using Digital Shortlne Analysis System

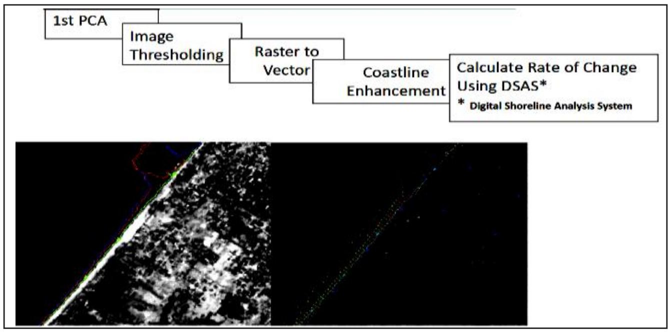

Fig. 13: Changing Rate Measurement through Arabia Coastline

Principal Component Analysis (PCA) [20] reduces the redundancy of multispectral facts based on the version and least correlation of each band. PCA is used as an enhancement operation or as a preprocessing procedure before the automated type of records. Predominant additives of the 3 IRS/LISS-III optical bands turned into correlated to deciding the band mixtures to stumble on the coastal side. Here, no band combination became observed to be useful for the coastal side discrimination without delay. Nonetheless, The Stable components of Band 2 and Band 4 tested, as this band mixture has shown the extra variance in the photo. Band 4 tested for the PCA photograph. From the PCA of LISS III Bands 2 and 4, The Total of 340,482 (42.6%) pixels had been classified as water [3] while 50% of pixels (numbering 399,627) had been classified as land and the ultimate 7.4% of pixels had classified as the transition zone. due to the fact, band 2 (0.57-0.61 µm) has high reflectance values for land functions, Whole the water our bodies soak up the NIR radiance, band 4 (0.72-0.82 µm). PCA suggests better consequences in delineating different land/water functions most effective, it became located unsuccessful within the transition zones.

VII. Changed Rating Measurements

The frameworks consequently gauge diverse factual boundaries, for example, the end of rating point (EPR) used to isolating the development of Coastline in a short line when estimation [1] occurs Remote sensing data. Long point rating (LPR) measured and controlled short line focuses on Coastline. Base line and short line plotted (Fig. 13). We measured EPR and LPR rates using QGIS (Fig. 14).

Shortlne mapping [17] designed direction between norths to south with classification of regions in EPR and LPR (Fig. 15). It classified as A, B, C, D in different colour mapping [19] for detecting changing rate. When sea level changes [16], Shortlne changes (Fig. 16 & 17) plotted using Dataset of real-time QGIS analysis [20].

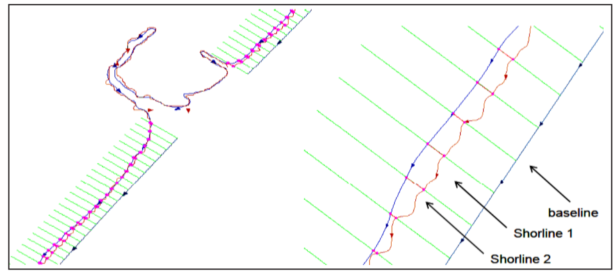

Fig. 14: Baseline and Short Line

Shorelines	Region	EPR (m/year)	LPR (m/year)
Shorelines 1987 – 2008 Image data set TM, ETM and SPOT	A (north Gaza)	-0.06	-0.32
	B (northern Seaport)	-0.26	-0.16
	C (southern Seaport)	0.98	0.8
	D (Wadi region)	-0.26	-0.36 *
	E (south Gaza)	0.32	0.3
	Entire shoreline	0.18	0.08
	Shoreline excluded region C	0.04	- 0.05

Fig. 15: Regions in EPR and LPR

Shorelines	Region	EPR
Shorelines 2002 – 2008 SPOT	A (north Gaza)	- 0.14
	B (northern Seaport)	- 0.28
	C (southern Seaport)	1.9
	D (Wadi region)	0.25
	E (south Gaza)	- 0.12
	Entire shoreline	0.28
	Shoreline excluded region C	- 0.07

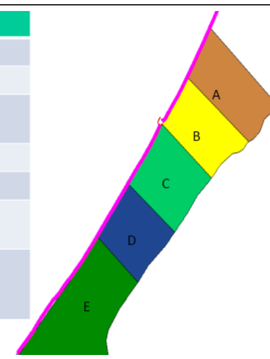

Fig. 16: Short Line between 2002-2008

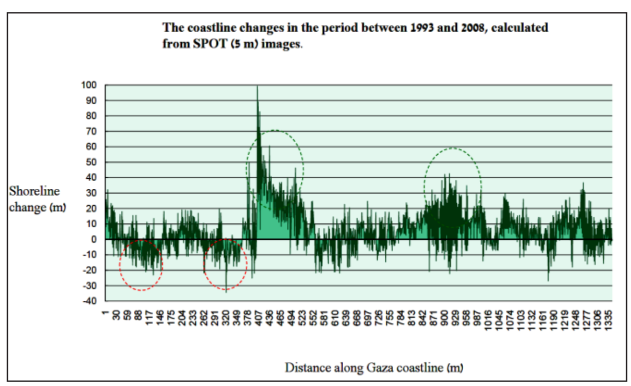

Fig. 17: Short Line Changes

VIII. Conclusion

The outcome shows a negative rate using QGIS software when all done, which implies that disintegration [14] has been the overwhelming cycle in the Arabia Coastal zone. Arabia waterfront zone can be partitioned into four locales as indicated by the paces of progress, which imported Short lines, baselines, region in EPR and LPR from SPOT images. Pace progress decreased in the beachfront zone when applying Multispectral images. The outcome of Negative rates coming from the north of Arabia and the Positive rate coming from the south of Arabia towards the seaport, which implies pressure movement of air circulation in the waterfront zone in the NE zone. Band Ratio and the main guidelines part could be utilized as a quick legitimate technique to separate the coastline. Medium goal pictures could be helpful to ascertain the seaside change in such a limited beachfront zone. Erosion [5] and Accretion rates had calculated using the Panchromatic Sharpened Algorithm and Universal Pixel Quality Index, Which implies classification of ATWT, DWT, GS, and PC. Multispectral images of the Coastal line are extracted and validated accuracy assessment. The changes in Coastal Shortlne and changes in baseline were detected. The Changing Rate through Arabia coastal line measured using a digital short-line analysis system.

References

[1] R. Benshila, G. Thoumyre, M. A. Najar, G. Abessolo, R. Almar, ... and D. Wilson, "A deep learning approach for estimation of the nearshore bathymetry," *J Coast Res*, vol. 95, no. sp1, pp. 1011-1015, May 2020.

[2] E. W. J. Bergsma, and R. Almar, "Coastal coverage of ESA's Sentinel 2 mission," *Adv Space Res*, vol. 65, no. 11, pp. 2636-2644, Jun. 2020. [Online]. Available: https://doi. org/10.1016/j.asr.2020.03.001

[3] I. Chawla, L. Karthikeyan, and A. K. Mishra, "A review of remote sensing applications for water security: Quantity, quality and extremes," *J Hydrol*, vol. 585, Jun. 2020, Art. no. 124826.

[4] R. A. M. Lauerburg, R. Diekmann, B. Blanz, K. Gee, R. Cormier, ... and V. Stelzenmüller, "Socio-ecological vulnerability to tipping points: A review of empirical approaches and their use for marine management," *Sci Total Environ*, vol. 705, Feb. 2020, Art. no. 135838.

[5] A. Toimil, P. Camus, I. J. Losada, G. L. Cozannet, R. J. Nicholls, D. Idier, and A. Maspataud, "Climate change driven coastal erosion modelling in temperate sandy beaches: Methods and uncertainty treatment," *Earth Sci Rev*, vol. 202, Mar. 2020, Art. no. 103110. [Online]. Available: https://doi.org/10.1016/j.earscirev. 2020.103110

[6] C. Viatte, C. Clerbaux, C. Maes, P. Daniel, R. Garello, S. Safeddine, and F. Ardhuin, "Air pollution and sea pollution seen from space," *Surv Geophys*, vol. 41, pp. 1583-1609, 2020. [Online]. Available: https://doi. org/10.1007/s10712-020-09599-0

[7] R. Almar, E. W. J. Bergsma, P. Maisongrande, and L. P. M. de Almeida, "Wave-derived coastal bathymetry from satellite video imagery: A showcase with pleiades persistent mode," *Remote Sens Environ*, vol. 231, 2019, Art. no. 111263. [Online]. Available: https://doi. org/10.1016/J.RSE.2019.111263

[8] L. P. Almeida, R. Almar, E. W. J. Bergsma, E. Berthier, P. Baptista, E. Garel, O. A. Dada, and B. Alves, "Deriving high spatial-resolution coastal topography from sub-meter satellite stereo imagery," *Remote Sens*, vol. 11, no. 5, 2019, Art. no. 590. [Online]. Available: https:// doi.org/10.3390/rs11050590

[9] F. Ardhuin, J. E. Stopa, B. Chapron, F. Collard, R. Husson, R. E. Jensen, J. Johannessen, A. Mouche, M. Passaro, G. D. Quartly, V. Swail, and I. Young, "Observing sea states," *Front Mar Sci* , vol. 6, 2019, Art. no. 124. [Online]. Available: https://doi. org/10.3389/ fmars.2019.00124

[10] G. Beaugrand, A. Conversi, A. Atkinson, J. Cloern, S. Chiba, S. Fonda-Umani, R. R. Kirby, C. H. Greene, E. Goberville, S. A. Otto, P. C. Reid, L. Stemmann, and M. Edwards, "Prediction of unprecedented biological shifts in the global ocean," *Nat Clim Change*, vol. 9, no. 3, pp. 237-243, 2019. [Online]. Available: https:// doi.org/10.1038/s41558-019-0420-1

[11] D. R. Bellwood, M. S. Pratchett, T. H. Morrison, G. G. Gurney, T. P. Hughes, J. G. Álvarez-Romero, J. C. Day, R. Grantham, A. Grech, and A. S. Hoey, "Coral reef conservation in the Anthropocene: Confronting spatial mismatches and prioritizing functions," *Biol Cons*, vol. 236, pp. 604-615, Aug. 2019. [Online]. Available: https://doi.org/10.1016/j.bioco n.2019.05.056

[12] N. Bindof et al., "Changing ocean, marine ecosystems, and dependent communities," in *IPCC Special Report on the Ocean and Cryosphere in a Changing Climate*, 2019.

[13] I. Caballero, and R. P. Stumpf, "Retrieval of nearshore bathymetry from Sentinel-2A and 2B satellites in South Florida coastal waters," *Estuar Coast Shelf Sci*, vol. 226, 2019, Art. no. 106277. [Online]. Available: https:// doi.org/10.1016/j. ecss.2019.106277

[14] F. Cian, J. M. Delgado Blasco, and L. Carrera, "Sentinel-1 for monitoring land subsidence of coastal cities in Africa using PSInSAR: A methodology based on the integration of SNAP and StaMPS," *Geosciences*, vol. 9, no. 3, 2019, Art. no. 124. [Online]. Available: https://doi.org/10.3390/geosciences9030124

[15] C. Corbau, U. Simeoni, C. Zoccarato, G. Mantovani, and P. Teatini, "Coupling land use evolution and subsidence in the Po Delta, Italy: Revising the past occurrence and prospecting the future management challenges," *Sci Total Environ,* vol. 654, pp. 1196-1208, 2019. [Online]. Available: https://doi.org/10.1016/j. scitotenv.2018.11.104

[16] G. Dodet, A. Melet, F. Ardhuin, X. Bertin, D. Idier, and R. Almar, "The contribution of wind-generated waves to coastal sea-level changes," *Surv Geophys*, vol. 40, no. 6, pp. 1563-1601, 2019. [Online]. Available: https://doi.org/10.1007/s1071 2-019-09557-5

[17] E. G. Evagorou, C. Mettas, A. Agapiou, K. Themistocleous, and D. G. Hadjimitsis, "Bathymetric maps from multi-temporal analysis of Sentinel-2 data: The case study of Limassol, Cyprus," *Adv. Geosci.,* vol. 45, pp. 397-407, 2019.

[18] E. B. Goldstein, G. Coco, and N. G. Plant, "A review of machine learning applications to coastal sediment transport and morphodynamics," *Earth Sci Rev*, vol. 194, pp. 97-108, 2019. [Online]. Available: https://doi.org/10.1016/j.earsc irev.2019.04

[19] F. Guerrini, L. Mari, and R. Casagrandi, "Modeling plastics exposure for the marine biota: Risk maps for fin whales in the Pelagos Sanctuary (North-Western Mediterranean)," *Frontiers in Marine Science*, 2019. [Online]. Available: https://doi.org/10.3389/fmars.2019.00299

[20] H. Hersbach, B. Bell, P. Berrisford, A. Horányi, J. Muñoz Sabater, J. Nicolas, R. Radu, D. Schepers, A. Simmons, C. Soci, and D. Dee, "Global reanalysis: Goodbye ERA-interim, hello ERA5," *ECMWF Newsletter,* No. 159, pp. 17-24, 2019. [Online]. Available: http://dx.doi.org/10.21957/vf291hehd7